

PointGroup: Dual-Set Point Grouping for 3D Instance Segmentation

Li Jiang^{1*} Hengshuang Zhao^{1*} Shaoshuai Shi¹ Shu Liu² Chi-Wing Fu¹ Jiaya Jia^{1,2}

¹The Chinese University of Hong Kong ²SmartMore

{lijiang, hszhao, cwfu, leojia}@cse.cuhk.edu.hk sssshi@ee.cuhk.edu.hk sliu@smartmore.com

Abstract

Instance segmentation is an important task for scene understanding. Compared to the fully-developed 2D, 3D instance segmentation for point clouds have much room to improve. In this paper, we present *PointGroup*, a new end-to-end bottom-up architecture, specifically focused on better grouping the points by exploring the void space between objects. We design a two-branch network to extract point features and predict semantic labels and offsets, for shifting each point towards its respective instance centroid. A clustering component is followed to utilize both the original and offset-shifted point coordinate sets, taking advantage of their complementary strength. Further, we formulate the *ScoreNet* to evaluate the candidate instances, followed by the *Non-Maximum Suppression (NMS)* to remove duplicates. We conduct extensive experiments on two challenging datasets, *ScanNet v2* and *S3DIS*, on which our method achieves the highest performance, 63.6% and 64.0%, compared to 54.9% and 54.4% achieved by former best solutions in terms of *mAP* with *IoU* threshold 0.5.

1. Introduction

Instance segmentation is a fundamental and challenging task that requires to predict not only the semantic labels but also the instance IDs for every object in the scene. It has drawn much interest recently, given the potential applications for both outdoor and indoor environment regarding autonomous driving, robot navigation, to name a few.

Convolutional neural networks has boosted the performance of 2D instance segmentation [10, 17, 29, 5]. However, given unordered and unstructured 3D point clouds, 2D methods cannot be directly extended to 3D points and make the latter remains very challenging [49, 19, 53]. In this paper, we address the challenging 3D point cloud instance segmentation task by exploring the void space between 3D objects, along with the semantic information, to better segment individual objects.

*Equal Contribution.

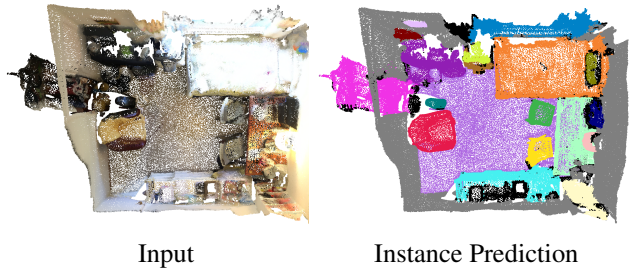


Figure 1: Example of 3D instance segmentation by our method from *ScanNet v2*. Instances are in different colors.

Specifically, we design a bottom-up end-to-end framework named *PointGroup* for 3D instance segmentation, with the key target of better grouping of points. Our pipeline is to first extract per-point semantic prediction and conduct efficient point grouping to harvest candidate object instances. We utilize a semantic segmentation backbone to extract descriptive features and predict a semantic label for each point. Parallel to the segmentation head, we adopt an offset branch to learn a relative offset to bring each point to its respective ground-truth instance centroid. By this means, we shift points of the same object instance towards the same centroid and gather them closer, thus enabling better grouping of points into objects and separation of nearby objects of the same class.

With the predicted semantic labels and offsets, we then adopt a simple and yet effective algorithm to group points into clusters. For each point, we take its coordinates as a reference, group it with nearby points of the same label, and expand the group progressively. Importantly, we consider two coordinate sets in two separate passes – the original point positions and those shifted by the predicted offsets. We call the process “Dual-Set Point Grouping.” The two types of results complement each other for accomplishing better performance. Further, we design the *ScoreNet* to evaluate and pick candidate groups. Non-maximum suppression is finally adopted to remove duplicate predictions.

We conduct extensive experiments on the challenging *ScanNet v2* [8] and *S3DIS* [2] datasets. *PointGroup* achieves the highest accuracy on both of them. For *Scan-*

Net v2, our performance on the test set is 63.6% in terms of mAP₅₀, which is 8.7% higher than the former best solution [23]. For S3DIS, we accomplish 64.0% mAP₅₀, 69.6% mPrec₅₀, and 69.2% mRec₅₀, outperforming all previous approaches by a large margin.

In summary, our contribution is threefold.

- We propose a bottom-up 3D instance segmentation framework, named *PointGroup*, to deal with the challenging 3D instance segmentation task.
- We propose a point clustering method based on dual coordinate sets, *i.e.*, the original and shifted sets. Along with the new ScoreNet, object instances can be better segmented out.
- The proposed method achieves state-of-the-art results on various challenging datasets, demonstrating its effectiveness and generality.

2. Related Work

Deep Learning in 3D Scenes 2D image pixels are in regular grids, thus can be naturally processed by convolutional neural networks [24, 22, 42, 46, 18]. In contrast, 3D point clouds are unordered and scattered in 3D space, causing extra difficulty in point cloud scene understanding [37, 41].

Several approaches handle data irregularity. The Multi-Layer Perception (MLP)-style networks, *e.g.*, PointNet [35, 37], directly apply MLP together with max-pooling to grab local and global structures in 3D. The learned features are then used for point cloud classification and segmentation. Other approaches [51, 48, 57, 52, 21] enhance feature learning on local regions by dynamic context aggregation and attention modules.

Besides working directly on the irregular input, several approaches transform the unordered point set to an ordered one to apply the convolution operations. PointCNN [26] learns the order transformation for points reweighting and permutation. Some other approaches [30, 43, 47, 39, 13, 7] align and voxelize point cloud to produce regular 3D ordered tensors for 3D convolution. Multi-view strategies [36, 44, 45] are also widely explored, where 3D point clouds are projected into 2D views for view-domain processing.

2D Instance Segmentation Instance segmentation aims to find the foreground objects in a scene and mark each object instance with a unique label. Overall, there are two major lines. The first is detection- or top-down-based, which directly detects object instances. Early works [14, 15] use proposals from MCG [1] for feature extraction. Methods of [9, 10, 16] adopt pooled features for faster processing. Mask R-CNN [17] is widely known as an effective approach with the extra segmentation head in the detection framework, like Faster R-CNN [38]. Further works [29, 6, 5] enhance the feature learning for instance segmentation.

The other line is segmentation- or bottom-up-based, where pixel-level semantic segmentation is performed followed by grouping of pixels to find object instances. Zhang *et al.* [56, 55] utilize MRF for local patch merging. Arnab and Torr [3] use CRF. Bai and Urtasun [4] combine the classical watershed transform and deep learning to produce energy maps to distinguish among individual instances. Liu *et al.* [28] employ a sequence of neural networks to construct objects from pixels.

3D Instance Segmentation With available large-scale 3D labeled datasets [8, 2], instance segmentation of 3D point clouds becomes important. Similar to 2D cases, current 3D methods can also be grouped into two lines.

Detection-based methods extract 3D bounding boxes, and inside each box, utilize a mask learning branch to predict the object mask. Yang *et al.* [53] present the 3D-BoNet that directly predicts 3D bounding boxes and point-level masks simultaneously per instance. Li *et al.* [54] propose GSPN, which takes an analysis-by-synthesis strategy to generate proposals for instance segmentation. Hou *et al.* [19] combine multi-view RGB input with 3D geometry to jointly infer object bounding boxes and corresponding instance masks in an end-to-end manner.

Contrarily, segmentation-based methods predict the semantic labels, and utilize point embedding to group points into object instances. Wang *et al.* [49] design SGPN by clustering points based on the semantic segmentation predicted by backbones such as PointNet++. Liu and Furukawa [27] predict both the semantic labels and affinity between adjacent voxels in different scales to group instances. Phm *et al.* [33] develop a multi-task learning framework with a multi-value CRF model to jointly reason over both the semantic and instance labels. Wang *et al.* [50] learn a semantic-aware point-level instance embedding to benefit learning of both the semantic and instance tasks. Lahoud *et al.* [23] introduce a multi-task learning strategy where points of the same instance are grouped closer and different clusters are more separated from each other.

Different from the above methods, we present a new approach named *PointGroup* to tackle the 3D instance segmentation task. Our proposed model mainly contains two parts – that is, (i) learning to group points into different clusters based on their semantic predictions in both the original coordinate space and shifted coordinate space, and (ii) ScoreNet to learn to predict the score for selecting proper clusters. The overall framework is differentiable. It can be jointly optimized and trained in an end-to-end manner.

3. Our Method

3.1. Architecture Overview

To obtain instance-level segmentation labels for 3D objects, we consider two problems. The first is to separate

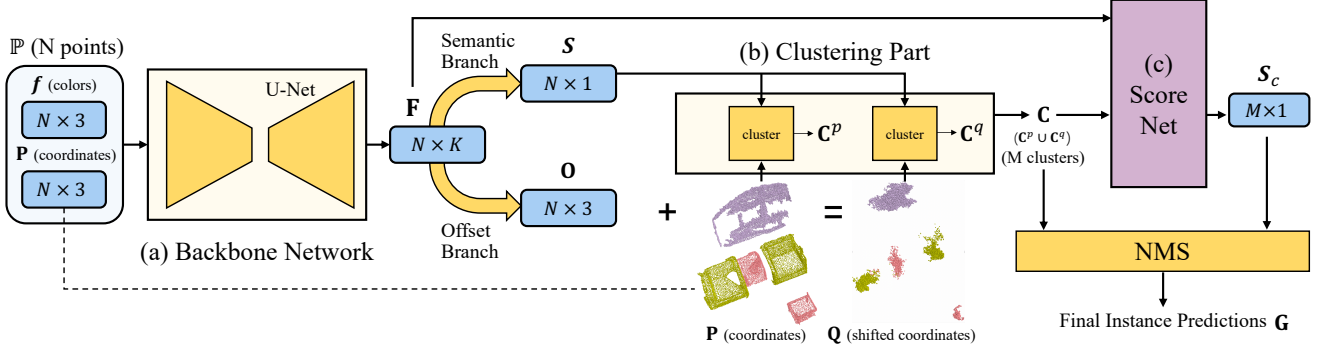


Figure 2: Illustration of the network architecture. It has three main components – (a) backbone network, (b) clustering part, and (c) ScoreNet. First, we use the backbone network to extract per-point features \mathbf{F} , followed by two branches to produce offset vectors $\mathbf{O} = \{o_i\}$ and semantic labels $\mathbf{S} = \{s_i\}$. Then, we introduce a clustering method to group points into candidate clusters on dual coordinate sets, *i.e.*, the original set \mathbf{P} and the shifted \mathbf{Q} , which produce \mathbf{C}^p and \mathbf{C}^q respectively. Lastly, we use ScoreNet to produce cluster scores \mathbf{S}_c . The set of color $\mathbf{f} = \{f_i\}$ serves as the input feature to the backbone.

the contents in the 3D space into individual objects, and the second is to determine the semantic label of each object. Unlike 2D images, there is no view-occlusion problem in the 3D scenes, and objects scattered in 3D are usually naturally separated by void space. Hence, we propose leveraging these characteristics of 3D objects to group 3D content into object instances according to the semantic information. Fig. 2 overviews the architecture of our approach, which has three main components, *i.e.*, the backbone, the point clustering part, and ScoreNet.

The input to the backbone network (Fig. 2(a)) is a point set \mathbb{P} of N points. Each point has a color $f_i = (r_i, g_i, b_i)$ and 3D coordinates $p_i = (x_i, y_i, z_i)$, where $i \in \{1, \dots, N\}$. The backbone extracts feature F_i for each point. We denote the output feature of the backbone as $\mathbf{F} = \{F_i\} \in \mathbb{R}^{N \times K}$, where K is the number of channels. We then feed \mathbf{F} into two branches, one for semantic segmentation and the other for predicting a per-point offset vector to shift each point towards the centroid of its respective object instance. Let s_i and $o_i = (\Delta x_i, \Delta y_i, \Delta z_i)$ denote the predicted semantic label and offset vector of point i , respectively.

After obtaining the semantic labels, we begin to group points into instance clusters based on the void space between objects. In the point clustering part (Fig. 2(b)), we introduce a clustering method to group points that are close to each other into the same cluster, if they have the same semantic label. However, clustering directly based on the point coordinate set $\mathbf{P} = \{p_i\}$ may fail to separate same-category objects that are close to each other in the 3D space and mis-group them, for example, two pictures that hang side-by-side on the wall.

Thus, we use the learned offset o_i to shift point i towards its respective instance centroid and obtain the shifted coordinates $q_i = p_i + o_i \in \mathbb{R}^3$. For points belonging to the same object instance, different from p_i , the shifted coordinates q_i

clutter around the same centroid. So by clustering based on shifted coordinate set $\mathbf{Q} = \{q_i\}$, we separate nearby objects better, even though they have the same semantic labels.

However, for points near object boundary, the predicted offsets may not be accurate. So, our clustering algorithm employs “dual” point coordinate sets, *i.e.*, the original coordinates \mathbf{P} and the shifted coordinates \mathbf{Q} . We denote the clustering results \mathbf{C} as the union of $\mathbf{C}^p = \{C_1^p, \dots, C_{M_p}^p\}$ and $\mathbf{C}^q = \{C_1^q, \dots, C_{M_q}^q\}$, which are the clusters discovered based on \mathbf{P} and \mathbf{Q} , respectively. Here, M_p and M_q denote the number of clusters in \mathbf{C}^p and \mathbf{C}^q , respectively, and $M = M_p + M_q$ denotes the total.

Lastly, we construct the ScoreNet (Fig. 2(c)) to process the proposed point clusters $\mathbf{C} = \mathbf{C}^p \cup \mathbf{C}^q$ and produce a score per cluster proposal. NMS is then applied to these proposals with the scores to generate final instance prediction. In the following, we denote the instance predictions as $\mathbf{G} = \{G_1, \dots, G_{M_{pred}}\} \subseteq \mathbf{C}$ and the ground-truth instances as $\mathbf{I} = \{I_1, \dots, I_{M_{gt}}\}$. Here, G_i and I_i are subsets of \mathbb{P} , while M_{pred} and M_{gt} denote the number of instances in \mathbf{G} and \mathbf{I} , respectively. Also, we use N_i^I and N_i^G to represent the number of points in I_i and G_i , respectively.

3.2. Backbone Network

We may use any point feature extraction network to serve as the backbone network (Fig. 2(a)). In our implementation, we voxelize the points and follow the procedure of [13] to construct a U-Net [25, 40] with Submanifold Sparse Convolution (SSC) and Sparse Convolution (SC). We then recover points from voxels to obtain the point-wise features. The contextual and geometric information is well extracted by the U-Net, which provides discriminative point-wise features \mathbf{F} for subsequent processing. Afterwards, we construct two branches based on the point-wise features \mathbf{F} to predict semantic label s_i and offset vector o_i for each point.

Semantic Segmentation Branch We apply an MLP to \mathbf{F} to produce semantic scores $\mathbf{SC} = \{sc_1, \dots, sc_N\} \in \mathbb{R}^{N \times N_{class}}$ for the N points over the N_{class} classes, and regularize the results by a cross entropy loss L_{sem} . The predicted semantic label s_i for point i is the class with the maximum score, *i.e.*, $s_i = \text{argmax}(sc_i)$.

Offset Prediction Branch The offset branch encodes \mathbf{F} to produce N offset vectors $\mathbf{O} = \{o_1, \dots, o_N\} \in \mathbb{R}^{N \times 3}$ for the N points. For points belonging to the same instance, we constrain their learned offsets by an L_1 regression loss as

$$L_{o_reg} = \frac{1}{\sum_i m_i} \sum_i \|o_i - (\hat{c}_i - p_i)\| \cdot m_i, \quad (1)$$

where $\mathbf{m} = \{m_1, \dots, m_N\}$ is a binary mask. $m_i = 1$ if point i is on an instance and $m_i = 0$ otherwise. \hat{c}_i is the centroid of the instance that point i belongs to, *i.e.*,

$$\hat{c}_i = \frac{1}{N_{g(i)}^I} \sum_{j \in I_{g(i)}} p_j, \quad (2)$$

where $g(i)$ maps point i to the index of its corresponding ground-truth instance, *i.e.*, the instance that contains point i . $N_{g(i)}^I$ is the number of points in instance $I_{g(i)}$.

The above mechanism looks similar to the vote generation strategy in VoteNet [34]. However, rather than regressing the bounding boxes based on the votes of a few subsampled seed points, we predict an offset vector per point to gather the instance points around a common instance centroid, in order to better cluster relevant points into the same instance. Also, we observe that the distances from points to their instance centroids usually have small values (0 to 1m). Fig. 3b gives the statistical analysis on the distribution of such distances in the ScanNet dataset. Considering diverse object sizes of different categories, we find it is hard for the network to regress precise offsets, particularly for boundary points of large-size objects, since these points are relatively far from the instance centroids. To address this issue, we formulate a direction loss to constrain the direction of predicted offset vectors. We follow [23] to define the loss as a means of minus cosine similarities, *i.e.*,

$$L_{o_dir} = - \frac{1}{\sum_i m_i} \sum_i \frac{o_i}{\|o_i\|_2} \cdot \frac{\hat{c}_i - p_i}{\|\hat{c}_i - p_i\|_2} \cdot m_i. \quad (3)$$

Such loss is irrelevant to the offset vector norm and ensures that the points move towards their instance centroids.

3.3. Clustering Algorithm

Given the predicted semantic labels and offset vectors, we are ready to group the input points into instances. To this end, we introduce a simple and yet effective clustering algorithm. It is detailed in Algorithm 1.

Algorithm 1 Clustering algorithm. N is the number of points. M is the number of clusters found by the algorithm.

Input: clustering radius r ;

cluster point number threshold N_θ ;

coordinates $\mathbf{X} = \{x_1, x_2, \dots, x_N\} \in \mathbb{R}^{N \times 3}$; and

semantic labels $\mathbf{S} = \{s_1, \dots, s_N\} \in \mathbb{R}^N$.

Output: clusters $\mathbf{C} = \{C_1, \dots, C_M\}$.

- 1: initialize an array v (visited) of length N with all zeros
 - 2: initialize an empty cluster set \mathbf{C}
 - 3: **for** $i = 1$ to N **do**
 - 4: **if** s_i is a stuff class (*e.g.*, wall) **then**
 - 5: $v_i = 1$
 - 6: **for** $i = 1$ to N **do**
 - 7: **if** $v_i == 0$ **then**
 - 8: initialize an empty queue Q
 - 9: initialize an empty cluster C
 - 10: $v_i = 1$; $Q.enqueue(i)$; add i to C
 - 11: **while** Q is not empty **do**
 - 12: $k = Q.dequeue()$
 - 13: **for** $j \in [1, N]$ with $\|x_j - x_k\|_2 < r$ **do**
 - 14: **if** $s_j == s_k$ and $v_j == 0$ **then**
 - 15: $v_j = 1$; $Q.enqueue(j)$; add j to C
 - 16: **if** number of points in $C > N_\theta$ **then**
 - 17: add C to \mathbf{C}
 - 18: **return** \mathbf{C}
-

The core step of our algorithm is that for point i , we get points within the ball of radius r centered at x_i (the coordinate of point i) and group points with the same semantic labels as point i into the same cluster. Here, r serves as a spatial constraint in the clustering, so that two intra-category objects at a distance larger than r are not grouped. Here, we use the breadth-first search to group points of the same instance into a cluster. In our implementation, for points in the scene, neighboring points within an r -sphere can be found in parallel in advance of the clustering to boost speed.

As presented in Sec. 3.1, we apply the clustering algorithm separately on the “dual” set, *i.e.*, the original coordinate set \mathbf{P} and the shifted set \mathbf{Q} , to produce cluster sets \mathbf{C}^p and \mathbf{C}^q . Clustering on \mathbf{P} may mis-group nearby objects of the same class, while clustering on \mathbf{Q} does not have this problem but may fail to handle the boundary points of large objects. We collectively employ \mathbf{P} and \mathbf{Q} to find candidate clusters due to their complementary properties. Analysis on the clustering performance of using \mathbf{P} alone, \mathbf{Q} alone, or both \mathbf{P} and \mathbf{Q} is presented in Sec. 4.2.2.

3.4. ScoreNet

The input to ScoreNet is the set of candidate clusters $\mathbf{C} = \{C_1, \dots, C_M\}$, where M denotes the total number of candidate clusters, and C_i denotes the i -th cluster. Also, we use N_i to represent the number of points in C_i . The goal of

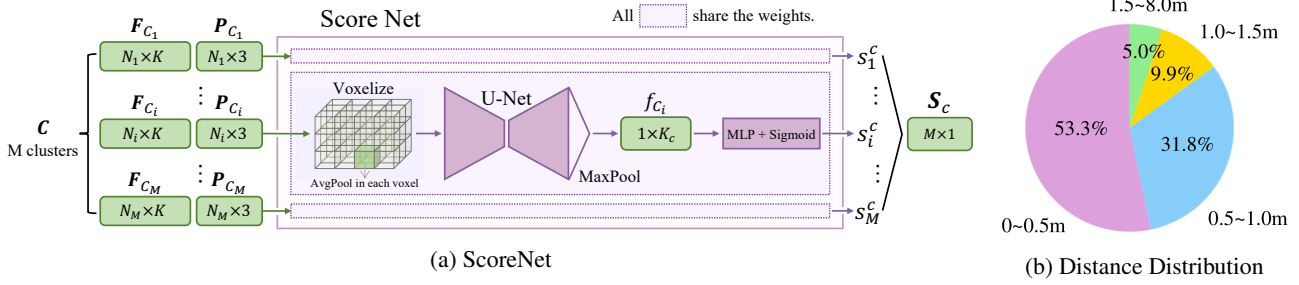


Figure 3: (a) Structure of ScoreNet. (b) Distribution of distances from points to their respective instance centroids in the ScanNet dataset [8] (including the training and validation sets).

ScoreNet is to predict a score for each cluster to indicate the quality of the associated cluster proposal, so that we could precisely reserve the better clusters in NMS and thus combine strength of \mathbf{C}^p and \mathbf{C}^q .

To start, for each cluster, we gather the point features from $\mathbf{F} \in \mathbb{R}^{N \times K}$ (the features extracted by the backbone) and form $\mathbf{F}_{C_i} = \{F_{h(C_i,1)}, \dots, F_{h(C_i,N_i)}\}$ for cluster C_i , where h maps the point index in C_i to corresponding point index in \mathbb{P} . Similarly, we express the coordinates for points in C_i as $\mathbf{P}_{C_i} = \{p_{h(C_i,1)}, \dots, p_{h(C_i,N_i)}\}$.

To better aggregate the cluster information, we take \mathbf{F}_{C_i} and \mathbf{P}_{C_i} as the initial features and coordinates, and voxelize the clusters the same way as we do at the beginning of the backbone network. The feature for each voxel is average-pooled from the initial features of points in that voxel. We then feed them into a small U-Net with SSC and SC to further encode the features. A cluster-aware max-pooling is then followed to produce a single cluster feature vector $f_{C_i} \in \mathbb{R}^{1 \times K_c}$ per cluster. The final cluster scores $\mathbf{S}_c = \{s_1^c, \dots, s_M^c\} \in \mathbb{R}^M$ are obtained as

$$\mathbf{S}_c = \text{Sigmoid}(\text{MLP}(\mathbf{F}_C)), \quad (4)$$

where $\mathbf{F}_C = \{f_{C_1}, \dots, f_{C_M}\} \in \mathbb{R}^{M \times K_c}$. The structure of ScoreNet is illustrated in Fig. 3a.

Inspired by [25, 20], to reflect the quality of clusters in the scores, we use a soft label to replace a binary 0/1 label to supervise the predicted cluster score as

$$\hat{s}_i^c = \begin{cases} 0 & iou_i < \theta_l \\ 1 & iou_i > \theta_h \\ \frac{1}{\theta_h - \theta_l} \cdot (iou_i - \theta_l) & \text{otherwise} \end{cases}, \quad (5)$$

where θ_l and θ_h are empirically set to 0.25 and 0.75 respectively in our implementation, and iou_i is the largest Intersection over Union (IoU) between cluster C_i and ground-truth instances as

$$iou_i = \max(\{\text{IoU}(C_i, I_j) \mid I_j \in \mathbf{I}\}). \quad (6)$$

We then use the binary cross-entropy loss as our score loss,

which is formulated as

$$L_{c_score} = -\frac{1}{M} \sum_{i=1}^M (\hat{s}_i^c \log(s_i^c) + (1 - \hat{s}_i^c) \log(1 - s_i^c)). \quad (7)$$

3.5. Network Training and Inference

Training We train the whole framework in an end-to-end manner with the total loss as

$$L = L_{sem} + L_{o_dir} + L_{o_reg} + L_{c_score}. \quad (8)$$

Inference In the inference process, we perform NMS on clusters \mathcal{C} with predicted scores \mathbf{S}_c to obtain the final instance predictions $\mathbf{G} \subseteq \mathcal{C}$. The IoU threshold is empirically set as 0.3. Since we cluster based on the semantic information, the semantic label of a cluster is exactly the category that the cluster points belong to.

4. Experiments

Our proposed PointGroup architecture is effective for instance segmentation of 3D point clouds. To demonstrate its effectiveness, we conduct extensive experiments on two challenging point cloud datasets, ScanNet v2 [8] and S3DIS [2]. On both of them, we achieve state-of-the-art performance on the 3D instance segmentation task.

4.1. Experimental Setting

Datasets The ScanNet v2 [8] dataset contains 1,613 scans with 3D object instance annotations. The dataset is split into training, validation, and testing sets, each with 1,201, 312, and 100 scans, respectively. 18 object categories are used for instance segmentation evaluation. For ablation studies, we train on the training set and report results on the validation set. To compare with other approaches, we train on the training set and report results on the testing set.

The S3DIS [2] dataset has 3D scans across six areas with 271 scenes in total. Each point is assigned one label out of 13 semantic classes. All the 13 classes are used in instance

Method	Avg AP ₅₀	bathub	bed	bookshe.	cabinet	chair	counter	curtain	desk	door	otherfu.	picture	refrige.	s. curtain	sink	sofa	table	toilet	window
SGPN [49]	0.143	0.208	0.390	0.169	0.065	0.275	0.029	0.069	0.000	0.087	0.043	0.014	0.027	0.000	0.112	0.351	0.168	0.438	0.138
3D-BEVIS [11]	0.248	0.667	0.566	0.076	0.035	0.394	0.027	0.035	0.098	0.099	0.030	0.025	0.098	0.375	0.126	0.604	0.181	0.854	0.171
R-PointNet [54]	0.306	0.500	0.405	0.311	0.348	0.589	0.054	0.068	0.126	0.283	0.290	0.028	0.219	0.214	0.331	0.396	0.275	0.821	0.245
DPC [12]	0.355	0.500	0.517	0.467	0.228	0.422	0.133	0.405	0.111	0.205	0.241	0.075	0.233	0.306	0.445	0.439	0.457	0.974	0.23
3D-SIS [19]	0.382	1.000	0.432	0.245	0.190	0.577	0.013	0.263	0.033	0.320	0.240	0.075	0.422	0.857	0.117	0.699	0.271	0.883	0.235
MASC [27]	0.447	0.528	0.555	0.381	0.382	0.633	0.002	0.509	0.260	0.361	0.432	0.327	0.451	0.571	0.367	0.639	0.386	0.980	0.276
PanopticFusion [32]	0.478	0.667	0.712	0.595	0.259	0.550	0.000	0.613	0.175	0.250	0.434	0.437	0.411	0.857	0.485	0.591	0.267	0.944	0.35
3D-BoNet [53]	0.488	1.000	0.672	0.590	0.301	0.484	0.098	0.620	0.306	0.341	0.259	0.125	0.434	0.796	0.402	0.499	0.513	0.909	0.439
MTML [23]	0.549	1.000	0.807	0.588	0.327	0.647	0.004	0.815	0.180	0.418	0.364	0.182	0.445	1.000	0.442	0.688	0.571	1.000	0.396
PointGroup (Ours)	0.636	1.000	0.765	0.624	0.505	0.797	0.116	0.696	0.384	0.441	0.559	0.476	0.596	1.000	0.666	0.756	0.556	0.997	0.513

Table 1: 3D instance segmentation results on ScanNet v2 testing set with AP₅₀ scores. Our proposed PointGroup approach yields the highest average AP₅₀, outperforming all state-of-the-art methods by a large margin. All numbers are from the ScanNet benchmark on 15/11/2019.

evaluation. Overall, we evaluate our model under two settings: (i) Area 5 is adopted for testing, whereas all the others are used for training; and (ii) six-fold cross validation that each area is treated as the testing set once.

Evaluation Metrics We use the widely-adopted evaluation metric – mean average precision (mAP). Specifically, AP₂₅ and AP₅₀ denote the AP scores with IoU threshold set to 25% and 50%, respectively. Also, AP averages the scores with IoU threshold set from 50% to 95%, with a step size of 5%. Besides, approaches of [50, 53] reported performance of mean precision (mPrec) and mean recall (mRec) on S3DIS, we also include these results for comparison.

Implementation Details We set the voxel size as 0.02m. In the clustering part, we set the clustering radius r as 0.03m and the minimum cluster point number N_θ as 50. In the training process, we use the Adam solver with a base learning rate of 0.001. For each scene in the dataset, we set the maximum number of points as 250k, due to GPU memory limit. If the scene has more than 250k points, we randomly crop part of the scene and gradually adjust the crop size, according to the number of points in the cropped area. During the testing process, we feed the whole scene into the network without cropping.

Specifically, scenes in S3DIS have high point density. Some scenes are even with millions of points. Hence, for each S3DIS scene, we randomly sub-sample $\sim 1/4$ points before each cropping.

4.2. Evaluation on ScanNet

4.2.1 Benchmark Results

We first report performance of our PointGroup model on the testing set of ScanNet v2, as listed in Table 1. PointGroup accomplishes the highest AP₅₀ score of 63.6%, outperforming all previous methods by a large margin. Compared with the former best solution [23], which obtains 54.9% AP₅₀ score, our result is 8.7% higher (absolute) and 15.8% better (relative). For detailed results on each category, PointGroup ranks the 1st place in 13 out of 18 classes in total.

4.2.2 Ablation Studies

We conduct ablation studies on the ScanNet validation set to analyze the design and parameter choice in our PointGroup.

Clustering based on Different Coordinate Sets Table 2 shows the comparison using the original coordinates \mathbf{P} alone, the shifted coordinates \mathbf{Q} alone, and both \mathbf{P} and \mathbf{Q} in the clustering. Clustering on points with \mathbf{P} alone may mis-group two close objects with the same semantic label into the same instance. Hence, for categories, in which two objects are likely to be very close to each other (*e.g.*, chairs and pictures), clustering on \mathbf{P} alone does not perform well. Clustering on \mathbf{Q} solves the problem in part by gathering instance points around the instance centroids and enlarging the space between clusters. However, due to inaccuracy in offset prediction, especially for boundary points of large objects (*e.g.*, curtains and counters), clustering on \mathbf{Q} alone does not perform perfectly.

Fig. 4 shows the qualitative results with models trained with clusters from different coordinate sets – (i) \mathbf{P} only, (ii) \mathbf{Q} only, and (iii) both \mathbf{P} and \mathbf{Q} . We could observe that the problem in (i) is the mistakenly grouped pictures on the wall in one cluster. The case of (ii) successfully separates the pictures into individual instances. Nevertheless, it suffers from inaccuracy around the object boundary areas. The case of (iii) takes strength of both (i) and (ii). Clustering on dual point sets (both \mathbf{P} and \mathbf{Q}) along with the precise scores from ScoreNet to select the final instance clusters, we combine the advantages of clustering on \mathbf{P} and on \mathbf{Q} to attain the best performance.

Ablation on the Clustering Radius r We use different values of r in the clustering algorithm. The performance varies as shown in Table 3. A small r is sensitive to point density. The scan for an object may have inconsistent point density in different parts. Clustering with such an r may not be able to grow in low-density parts. On the contrary, a large r increases the risk of grouping two nearby same-class objects into one. We empirically set r to 0.03 (meter).

Method	Metric	mean	bathub	bed	booksh.	cabinet	chair	counter	curtain	desk	door	otherfu.	picture	refrige.	s. curtain	sink	sofa	table	toilet	window
Original P	AP	0.283	0.414	0.327	0.244	0.167	0.493	0.083	0.269	0.089	0.193	0.286	0.205	0.207	0.373	0.226	0.361	0.251	0.684	0.231
	AP ₅₀	0.507	0.692	0.647	0.481	0.347	0.685	0.231	0.508	0.308	0.384	0.453	0.359	0.301	0.632	0.537	0.660	0.531	0.961	0.413
	AP ₂₅	0.659	0.840	0.764	0.597	0.496	0.791	0.588	0.614	0.686	0.529	0.600	0.432	0.401	0.660	0.775	0.777	0.721	0.995	0.601
Shifted Q	AP	0.328	0.499	0.383	0.248	0.217	0.713	0.008	0.241	0.165	0.216	0.318	0.211	0.238	0.422	0.292	0.383	0.362	0.799	0.194
	AP ₅₀	0.529	0.738	0.694	0.550	0.435	0.884	0.035	0.389	0.410	0.413	0.501	0.363	0.366	0.617	0.590	0.648	0.571	0.948	0.375
	AP ₂₅	0.677	0.863	0.795	0.699	0.617	0.931	0.426	0.541	0.697	0.538	0.623	0.446	0.366	0.765	0.826	0.848	0.669	0.999	0.533
Both P & Q	AP	0.348	0.597	0.376	0.267	0.253	0.712	0.069	0.266	0.140	0.229	0.339	0.208	0.246	0.416	0.298	0.434	0.385	0.758	0.275
	AP ₅₀	0.569	0.805	0.696	0.549	0.481	0.877	0.224	0.449	0.416	0.420	0.530	0.377	0.372	0.644	0.611	0.715	0.629	0.983	0.462
	AP ₂₅	0.713	0.865	0.795	0.744	0.673	0.925	0.648	0.616	0.741	0.548	0.654	0.482	0.383	0.711	0.828	0.851	0.742	1.000	0.636

Table 2: Ablation results using different coordinate sets on the ScanNet v2 validation set. Adopting both the original and shifted coordinates for clustering yields the best 3D instance segmentation performance.



Figure 4: Instance predictions produced by models trained with clustering on (i) P only, (ii) shifted coordinates Q only, and (iii) both. The last column shows the predicted instances of (iii) represented with Q, where stuff points are ignored.

Method	avg AP	avg AP ₅₀	avg AP ₂₅
$r = 2\text{cm}$	0.285	0.501	0.651
$r = 3\text{cm}$	0.348	0.569	0.713
$r = 4\text{cm}$	0.337	0.552	0.700
$r = 5\text{cm}$	0.342	0.552	0.699

Table 3: Ablation results for clustering with different radii r on the ScanNet v2 validation set.

Ablation for the ScoreNet We also ablate the ScoreNet, which is used to evaluate the quality of each candidate cluster (see Sec.3.4). Here, we directly use the output scores from ScoreNet to rank instances for calculating the AP.

Apart from regressing the instance quality, an alternative way is to directly use the averaged semantic probability of the related instance category inside an instance as the quality confidence. By this means, the results in terms of AP/AP₅₀/AP₂₅ are 30.2/51.9/68.9(%), which are worse than those with ScoreNet where results are 34.8/56.9/71.3(%). This indicates that the proposed ScoreNet is vital and necessary for improving the instance segmentation results by providing precise scores for NMS.

4.2.3 Runtime Analysis

Our method takes a whole scene as input per pass. Its runtime depends on the number of points and scene complexity. For runtime analysis, we sampled four scenes randomly from the ScanNet v2 validation set and tested them 100 times on a Titan Xp GPU to get an average runtime per scene. Table 4 reports the runtime breakdown. Clustering

	#Points	Total Time	BB	Clustering on P and Q				SCN	NMS
				BQ _p	CL _p	BQ _q	CL _q		
1	239,261	865	332	95	16	95	70	176	82
2	45,557	261	177	5	2	5	5	52	14
3	186,857	567	281	44	9	45	31	95	62
4	60,071	271	180	6	3	7	15	55	6
avg	132,937	491	243	38	8	38	30	95	41

Table 4: Inference time (ms). BB denotes backbone + two branches; BQ denotes ballquery; subscripts p and q denote clustering on P and Q respectively; CL denotes our clustering algorithm; and SCN denotes ScoreNet.

Method	AP ₅₀	mPrec ₅₀	mRec ₅₀
SGPN [†] [49]	-	0.360	0.287
ASIS [†] [50]	-	0.553	0.424
PointGroup [†]	0.578	0.619	0.621
SGPN [‡] [49]	0.544	0.382	0.312
PartNet [‡] [31]	-	0.564	0.434
ASIS [‡] [50]	-	0.636	0.475
3D-BoNet [‡] [53]	-	0.656	0.476
PointGroup [‡]	0.640	0.696	0.692

Table 5: Instance segmentation results on the S3DIS validation set. Methods marked with [†] are evaluated on Area 5; those marked with [‡] are on the 6-fold cross validation.

on Q (shifted) usually takes more time than clustering on P (original), as shifted points could have more neighbors.

4.3. Evaluation on S3DIS

We also evaluate our proposed PointGroup model on the S3DIS dataset. Apart from adopting AP₅₀ as an evaluation

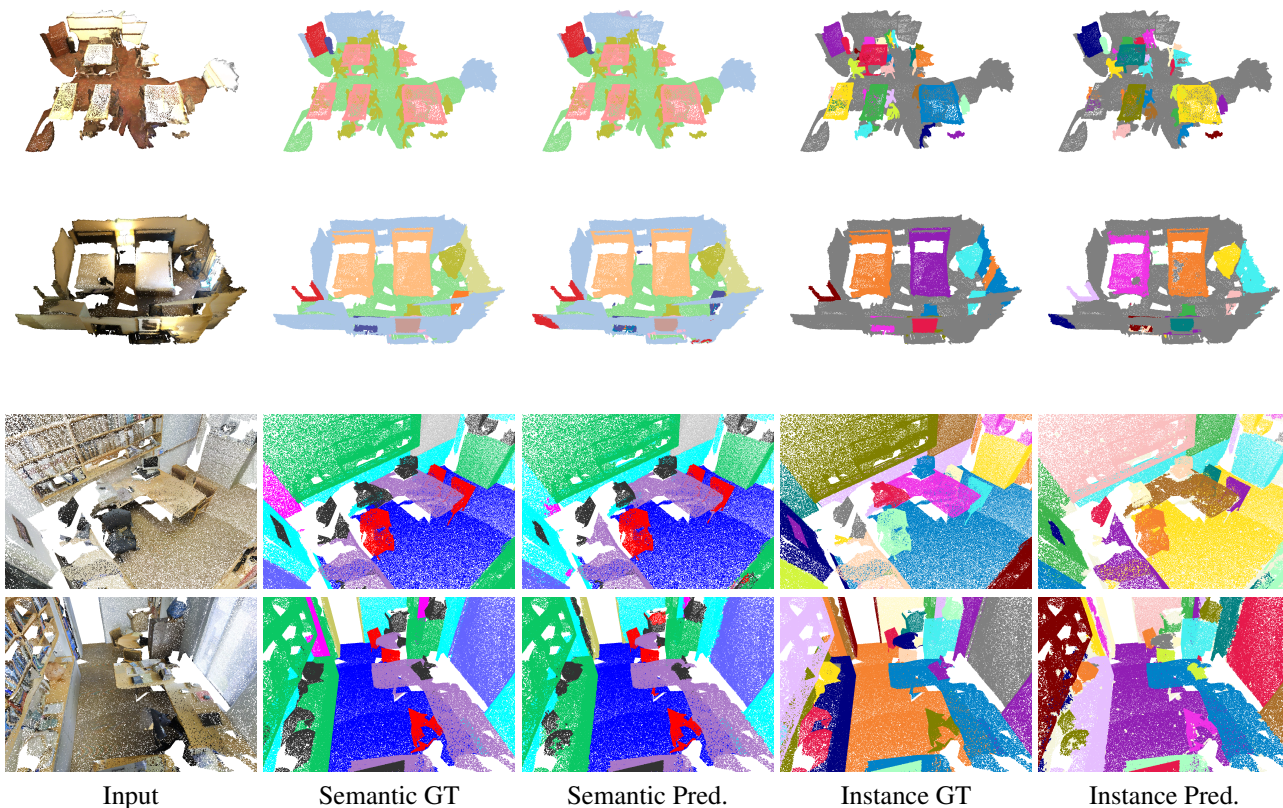


Figure 5: Visualization of the semantic and instance segmentation results on ScanNet v2 (top) and S3DIS (bottom). For instance predictions, different colors represent separate instances, and the semantic results indicate the categories of instances.

metric, we also include the $mPrec_{50}$ and $mRec_{50}$ results in Table 5, where we use a score threshold of 0.2 to remove some low-confidence clusters.

PointGroup reaches the highest performance in terms of all three evaluation metrics. For results on Area 5, PointGroup gets 57.8% on AP_{50} , 61.9% on $mPrec_{50}$ and 62.1% on $mRec_{50}$. The $mPrec_{50}$ and $mRec_{50}$ are 6.6 and 19.7 points higher than ASIS [50], respectively. For the results on 6-fold cross validation, PointGroup is 9.6 points higher than SGPN [49] regarding AP_{50} , which is a big margin. The $mPrec_{50}$ and $mRec_{50}$ scores are 4 and 21.6 points higher than the second-best solution [53].

The large improvement of PointGroup over the former best approaches across different challenging datasets demonstrate its effectiveness and generality. Several visual illustrations of PointGroup over these two datasets are included in Fig. 5. We observe that the proposed approach well captures the 3D geometry information and obtains precise instance segmentation masks.

5. Conclusion

We have proposed PointGroup for 3D instance segmentation, with a specific focus of better grouping points by

exploring the in-between space and point semantic labels among the object instances. Considering the situation that two intra-category objects may be very close to each other, we design a two-branch network to respectively learn a per-point semantic label and a per-point offset vector for moving each point towards its respective instance centroid. We then cluster points based on both the original point coordinates and the offset-shifted point coordinates. It combines the complementary strength of the two coordinate sets to optimize point grouping precision. Further, we introduced the ScoreNet to learn to evaluate the generated candidate clusters, followed by the NMS to avoid duplicates before we output the final predicted instances. PointGroup accomplished the best ever results.

In our future work, we plan to further introduce a progressive refinement module to relieve the semantic inaccuracy problem that affects the instance grouping and explore the possibility of incorporating weakly- or self-supervision techniques to further boost the performance.

Acknowledgments This project is supported in part by the Research Grants Council of the Hong Kong Special Administrative Region (Project no. CUHK 14201717).

References

- [1] Pablo Arbeláez, Jordi Pont-Tuset, Jonathan T Barron, Ferran Marques, and Jitendra Malik. Multiscale combinatorial grouping. In *CVPR*, 2014.
- [2] Iro Armeni, Ozan Sener, Amir R. Zamir, Helen Jiang, Ioannis Brilakis, Martin Fischer, and Silvio Savarese. 3D semantic parsing of large-scale indoor spaces. In *CVPR*, 2016.
- [3] Anurag Arnab and Philip HS Torr. Pixelwise instance segmentation with a dynamically instantiated network. In *CVPR*, 2017.
- [4] Min Bai and Raquel Urtasun. Deep watershed transform for instance segmentation. In *CVPR*, 2017.
- [5] Kai Chen, Jiangmiao Pang, Jiaqi Wang, Yu Xiong, Xiao-xiao Li, Shuyang Sun, Wansen Feng, Ziwei Liu, Jianping Shi, Wanli Ouyang, et al. Hybrid task cascade for instance segmentation. In *CVPR*, 2019.
- [6] Liang-Chieh Chen, Alexander Hermans, George Papandreou, Florian Schroff, Peng Wang, and Hartwig Adam. Masklab: Instance segmentation by refining object detection with semantic and direction features. In *CVPR*, 2018.
- [7] Christopher Choy, JunYoung Gwak, and Silvio Savarese. 4D spatio-temporal ConvNets: Minkowski convolutional neural networks. In *CVPR*, 2019.
- [8] Angela Dai, Angel X. Chang, Manolis Savva, Maciej Halber, Thomas Funkhouser, and Matthias Nießner. ScanNet: Richly-annotated 3D reconstructions of indoor scenes. In *CVPR*, 2017.
- [9] Jifeng Dai, Kaiming He, and Jian Sun. Convolutional feature masking for joint object and stuff segmentation. In *CVPR*, 2015.
- [10] Jifeng Dai, Kaiming He, and Jian Sun. Instance-aware semantic segmentation via multi-task network cascades. In *CVPR*, 2016.
- [11] Cathrin Elich, Francis Engelmann, Jonas Schult, Theodora Kontogianni, and Bastian Leibe. 3d-bevis: Birds-eye-view instance segmentation. *arXiv:1904.02199*, 2019.
- [12] Francis Engelmann, Theodora Kontogianni, and Bastian Leibe. Dilated point convolutions: On the receptive field of point convolutions. *arXiv:1907.12046*, 2019.
- [13] Benjamin Graham, Martin Engelcke, and Laurens van der Maaten. 3D semantic segmentation with submanifold sparse convolutional networks. In *CVPR*, 2018.
- [14] Bharath Hariharan, Pablo Arbeláez, Ross Girshick, and Jitendra Malik. Simultaneous detection and segmentation. In *ECCV*, 2014.
- [15] Bharath Hariharan, Pablo Andrés Arbeláez, Ross B. Girshick, and Jitendra Malik. Hypercolumns for object segmentation and fine-grained localization. In *CVPR*, 2015.
- [16] Zeeshan Hayder, Xuming He, and Mathieu Salzmann. Boundary-aware instance segmentation. In *CVPR*, 2017.
- [17] Kaiming He, Georgia Gkioxari, Piotr Dollár, and Ross Girshick. Mask R-CNN. In *ICCV*, 2017.
- [18] Kaiming He, Xiangyu Zhang, Shaoqing Ren, and Jian Sun. Deep residual learning for image recognition. In *CVPR*, 2016.
- [19] Ji Hou, Angela Dai, and Matthias Nießner. 3D-SIS: 3D semantic instance segmentation of RGB-D scans. In *CVPR*, 2019.
- [20] Borui Jiang, Ruixuan Luo, Jiayuan Mao, Tete Xiao, and Yunying Jiang. Acquisition of localization confidence for accurate object detection. In *ECCV*, 2018.
- [21] Li Jiang, Hengshuang Zhao, Shu Liu, Xiaoyong Shen, Chi-Wing Fu, and Jiaya Jia. Hierarchical point-edge interaction network for point cloud semantic segmentation. In *ICCV*, 2019.
- [22] Alex Krizhevsky, Ilya Sutskever, and Geoffrey E Hinton. Imagenet classification with deep convolutional neural networks. In *NIPS*, 2012.
- [23] Jean Lahoud, Bernard Ghanem, Marc Pollefeys, and Martin R Oswald. 3D instance segmentation via multi-task metric learning. In *ICCV*, 2019.
- [24] Yann LeCun, Léon Bottou, Yoshua Bengio, Patrick Haffner, et al. Gradient-based learning applied to document recognition. *IEEE*, 1998.
- [25] Buyu Li, Wanli Ouyang, Lu Sheng, Xingyu Zeng, and Xiaogang Wang. Gs3d: An efficient 3d object detection framework for autonomous driving. In *CVPR*, 2019.
- [26] Yangyan Li, Rui Bu, Mingchao Sun, Wei Wu, Xinhan Di, and Baoquan Chen. PointCNN: Convolution on \mathcal{X} -transformed points. In *NIPS*, 2018.
- [27] Chen Liu and Yasutaka Furukawa. MASC: Multi-scale affinity with sparse convolution for 3D instance segmentation. *arXiv:1902.04478*, 2019.
- [28] Shu Liu, Jiaya Jia, Sanja Fidler, and Raquel Urtasun. SGN: Sequential grouping networks for instance segmentation. In *ICCV*, 2017.
- [29] Shu Liu, Lu Qi, Haifang Qin, Jianping Shi, and Jiaya Jia. Path aggregation network for instance segmentation. In *CVPR*, 2018.
- [30] Daniel Maturana and Sebastian Scherer. VoxNet: A 3D convolutional neural network for real-time object recognition. In *IROS*, 2015.
- [31] Kaichun Mo, Shilin Zhu, Angel X Chang, Li Yi, Subarna Tripathi, Leonidas J Guibas, and Hao Su. Partnet: A large-scale benchmark for fine-grained and hierarchical part-level 3d object understanding. In *CVPR*, 2019.
- [32] Gaku Narita, Takashi Seno, Tomoya Ishikawa, and Yohsuke Kaji. PanopticFusion: Online volumetric semantic mapping at the level of stuff and things. In *IROS*, 2019.
- [33] Quang-Hieu Pham, Thanh Nguyen, Binh-Son Hua, Gemma Roig, and Sai-Kit Yeung. Jsis3d: Joint semantic-instance segmentation of 3d point clouds with multi-task pointwise networks and multi-value conditional random fields. In *CVPR*, 2019.
- [34] Charles R Qi, Or Litany, Kaiming He, and Leonidas J Guibas. Deep hough voting for 3d object detection in point clouds. In *ICCV*, 2019.
- [35] Charles Ruizhongtai Qi, Hao Su, Kaichun Mo, and Leonidas J. Guibas. PointNet: Deep learning on point sets for 3D classification and segmentation. In *CVPR*, 2017.
- [36] Charles R Qi, Hao Su, Matthias Nießner, Angela Dai, Mengyuan Yan, and Leonidas J Guibas. Volumetric and

- multi-view cnns for object classification on 3D data. In *CVPR*, 2016.
- [37] Charles Ruizhongtai Qi, Li Yi, Hao Su, and Leonidas J. Guibas. PointNet++: Deep hierarchical feature learning on point sets in a metric space. In *NIPS*, 2017.
- [38] Shaoqing Ren, Kaiming He, Ross Girshick, and Jian Sun. Faster R-CNN: Towards real-time object detection with region proposal networks. In *NIPS*, 2015.
- [39] Gernot Riegler, Ali Osman Ulusoy, and Andreas Geiger. OctNet: Learning deep 3D representations at high resolutions. In *CVPR*, 2017.
- [40] Olaf Ronneberger, Philipp Fischer, and Thomas Brox. U-net: Convolutional networks for biomedical image segmentation. In *MICCAI*, 2015.
- [41] Shaoshuai Shi, Xiaogang Wang, and Hongsheng Li. Pointcnn: 3d object proposal generation and detection from point cloud. In *CVPR*, 2019.
- [42] Karen Simonyan and Andrew Zisserman. Very deep convolutional networks for large-scale image recognition. In *ICLR*, 2015.
- [43] Shuran Song, Fisher Yu, Andy Zeng, Angel X Chang, Manolis Savva, and Thomas Funkhouser. Semantic scene completion from a single depth image. In *CVPR*, 2017.
- [44] Hang Su, Subhransu Maji, Evangelos Kalogerakis, and Erik G. Learned-Miller. Multi-view convolutional neural networks for 3D shape recognition. In *ICCV*, 2015.
- [45] Hao Su, Fan Wang, Eric Yi, and Leonidas J. Guibas. 3D-assisted feature synthesis for novel views of an object. *ICCV*, 2015.
- [46] Christian Szegedy, Wei Liu, Yangqing Jia, Pierre Sermanet, Scott Reed, Dragomir Anguelov, Dumitru Erhan, Vincent Vanhoucke, and Andrew Rabinovich. Going deeper with convolutions. In *CVPR*, 2015.
- [47] Lyne P. Tchammi, Christopher B. Choy, Iro Armeni, JunYoung Gwak, and Silvio Savarese. SEGCloud: Semantic segmentation of 3D point clouds. In *3DV*, 2017.
- [48] Shenlong Wang, Simon Suo, Wei-Chiu Ma, Andrei Pokrovsky, and Raquel Urtasun. Deep parametric continuous convolutional neural networks. In *CVPR*, 2018.
- [49] Weiyue Wang, Ronald Yu, Qiangui Huang, and Ulrich Neumann. SGP: Similarity group proposal network for 3D point cloud instance segmentation. In *CVPR*, 2018.
- [50] Xinlong Wang, Shu Liu, Xiaoyong Shen, Chunhua Shen, and Jiaya Jia. Associatively segmenting instances and semantics in point clouds. In *CVPR*, 2019.
- [51] Yue Wang, Yongbin Sun, Ziwei Liu, Sanjay E. Sarma, Michael M. Bronstein, and Justin M. Solomon. Dynamic graph CNN for learning on point clouds. *TOG*, 2019.
- [52] Wenxuan Wu, Zhongang Qi, and Li Fuxin. PointConv: Deep convolutional networks on 3D point clouds. In *CVPR*, 2019.
- [53] Bo Yang, Jianan Wang, Ronald Clark, Qingyong Hu, Sen Wang, Andrew Markham, and Niki Trigoni. Learning object bounding boxes for 3D instance segmentation on point clouds. In *NeurIPS*, 2019.
- [54] Li Yi, Wang Zhao, He Wang, Minhyuk Sung, and Leonidas J. Guibas. GSPN: Generative shape proposal network for 3D instance segmentation in point cloud. In *CVPR*, 2019.
- [55] Ziyu Zhang, Sanja Fidler, and Raquel Urtasun. Instance-level segmentation for autonomous driving with deep densely connected MRFs. In *CVPR*, 2016.
- [56] Ziyu Zhang, Alexander G Schwing, Sanja Fidler, and Raquel Urtasun. Monocular object instance segmentation and depth ordering with CNNs. In *ICCV*, 2015.
- [57] Hengshuang Zhao, Li Jiang, Chi-Wing Fu, and Jiaya Jia. PointWeb: Enhancing local neighborhood features for point cloud processing. In *CVPR*, 2019.